Identification of the monolayer thickness difference in a mechanically exfoliated thick flake of hexagonal boron nitride and graphite for van der Waals heterostructures

Hattori, Yoshiaki

Taniguchi, Takashi

Watanabe, Kenji

Kitamura, Masatoshi

(Citation)
Nanotechnology,34(29):295701

(Issue Date)
2023-07-16

(Resource Type)
journal article

(Version)
Version of Record

PAPER • **OPEN ACCESS**

Identification of the monolayer thickness difference in a mechanically exfoliated thick flake of hexagonal boron nitride and graphite for van der Waals heterostructures

To cite this article: Yoshiaki Hattori *et al* 2023 *Nanotechnology* **34** 295701

OPEN ACCESS
IOP Publishing
Nanotechnology

Nanotechnology **34** (2023) 295701 (10pp)
https://doi.org/10.1088/1361-6528/accf23

Identification of the monolayer thickness difference in a mechanically exfoliated thick flake of hexagonal boron nitride and graphite for van der Waals heterostructures

Yoshiaki Hattori[1,*], **Takashi Taniguchi**[2], **Kenji Watanabe**[3] and **Masatoshi Kitamura**[1,*]

[1] Department of Electrical and Electronic Engineering, Kobe University, 1-1, Rokkodai-cho, Nada, Kobe, 657-8501, Japan
[2] International Center for Materials Nanoarchitectonics, National Institute for Materials Science, 1-1 Namiki, Tsukuba 305-0044, Japan
[3] Research Center for Functional Materials, National Institute for Materials Science, 1-1 Namiki, Tsukuba 305-0044, Japan

E-mail: hattori@eedept.kobe-u.ac.jp and kitamura@eedept.kobe-u.ac.jp

Received 25 December 2022, revised 11 April 2023
Accepted for publication 21 April 2023
Published 9 May 2023

Abstract

Exfoliated flakes of layered materials, such as hexagonal boron nitride (hBN) and graphite with a thickness of several tens of nanometers, are used to construct van der Waals heterostructures. A flake with a desirable thickness, size, and shape is often selected from many exfoliated flakes placed randomly on a substrate using an optical microscope. This study examined the visualization of thick hBN and graphite flakes on SiO_2/Si substrates through calculations and experiments. In particular, the study analyzed areas with different atomic layer thicknesses in a flake. For visualization, the SiO_2 thickness was optimized based on the calculation. As an experimental result, the area with different thicknesses in a hBN flake showed different brightness in the image obtained using an optical microscope with a narrow band-pass filter. The maximum contrast was 12% with respect to the difference of monolayer thickness. In addition, hBN and graphite flakes were observed by differential interference contrast (DIC) microscopy. In the observation, the area with different thicknesses exhibited different brightnesses and colors. Adjusting the DIC bias had a similar effect to selecting a wavelength using a narrow band-pass filter.

Supplementary material for this article is available online

Keywords: hBN, graphite, 2D materials, optical interferometry, differential interference contrast microscopy

(Some figures may appear in colour only in the online journal)

1. Introduction

Van der Waals heterostructure devices constructed from layered materials of various substances have been studied intensively because of their novel electrical and optical properties. Layered materials can obtain an atomically flat, ideal interface and a precisely controlled number of layers.

* Authors to whom any correspondence should be addressed.

Van der Waals heterostructured devices are composed of a monolayer or layered materials several ten-nanometer thick. The typical materials are graphene, hexagonal boron nitride (hBN), and transition-metal dichalcogenide. The heterostructure is constructed by stacking exfoliated flakes using mechanical transfer techniques [1–7].

The exfoliated flakes are prepared from bulk crystals with adhesive tape [8]. After mechanical exfoliation, the flakes are transferred to a substrate. Since a large number of flakes with different size, shape, and thickness are placed randomly on a substrate, appropriate flakes for constructing a heterostructure are found in them. Generally, a large and flat isolated flake with the same number of layers is ideal for use in heterostructures. However, an exfoliated flake often has areas with different atomic layer thicknesses. In addition, residues of tapes for exfoliation are present on the flake surface. These disturb the construction of ideal interfaces in a heterostructure. Thus, an optical technique that can provide high contrast for finding ideal flakes is required for constructing a desirable heterostructure.

The presence of a flake of a layered material placed on a substrate can be visualized by optical microscopy from the difference between the reflection intensity from the flake surface and the substrate surface. In the first paper on mechanically exfoliated graphene, a thermally oxidized Si substrate with 300 nm-thick SiO_2 layer was employed for the visualization [8]. The visibility of an atomically thin flake depends on the thickness of SiO_2 layer by optical interference, where a 90- or 300 nm-thick SiO_2 provides a large difference in reflection intensity [9, 10]. Therefore, a thermally oxidized Si substrate with a 90 or 300 nm-thick SiO_2 layer has been commonly used in layer materials research.

The reflection intensity is discussed based on the reflectance (R) governed by interference effects. To visualize a flake of a layered material on a substrate, the optical contrast is defined as $C_n = (R_n - R_{sub})/R_{sub} = \Delta R/R_{sub} = R_n/R_{sub} - 1$ where n is the number of layers for the layered material, R_n is the reflectance for the surface of the flake, R_{sub} is the reflectance for the surface of the substrate, and $\Delta R = R_n - R_{sub}$. Since R_n and R_{sub} depend on wavelength (λ), the observation at a wavelength that R_{sub} is small leads to the visualization of a flake with high contrast [9–20]. For a Si substrate with a 90 or 300 nm-thick SiO_2 layer, R_{sub} is small in the visible wavelength range and ~10% at λ = ~550 nm [9, 10]. When observing a flake of n = 1–5, C_n increases linearly with n [13, 14]. Therefore, n can be estimated from the C_n value obtained by the observation.

Another issue is to observe the difference in n for a thick flake of $n > 5$. Although ΔR for a thick flake is large, it is difficult to recognize the difference in n for a flake since $(R_n - R_{n-1})/R_n$ is small. Hence, $(R_n - R_{n-1})/R_n$ rather than C_n is a suitable definition of contrast for the difference in n for a thick flake. Therefore, to visualize the difference in n, the thickness of a SiO_2 layer should be adjusted so that R_n is small.

Some groups have been studying the visualization of an ultra-thin film using a substrate with low reflectance, such as a $Au/SiO_2/Si$ [11, 12, 16–18] or SiN_x/Si substrate [15, 19, 20]. A monolayer (1 L) hBN flake can be visualized with high contrast using such a substrate. A transparent hBN flake with a 1 L thickness of 0.333 nm is generally difficult to visualize. One of the groups realized the C_1 = 12% for 1 L hBN using an optimized SiN_x/Si substrate with R_{sub} = ~0% at a certain λ. The C_1 = 12% value is larger than C_1 = 2.5% for an optimized SiO_2/Si substrate with R_{sub} = ~10% [15]. For a hBN flake with n atomic layer thickness, an area with a 1 L difference in the flake with high contrast might be observed by adjusting R_n to zero. Therefore, a study that intentionally reduces R_n to zero is needed to visualize an area with a thickness difference of a few atomic layers in a thick hBN flake.

This study investigated the visualization of thick hBN and graphite flakes placed on SiO_2/Si substrates by optical microscopy to visualize areas with different numbers of layers in a thick flake. A flake with a thickness of 4–100 nm is called a thick flake in this study. This is because hBN flakes, approximately 30 nm in thickness, and graphite flakes, a few nm in thickness, are used in van der Waals heterostructure devices [21–26]. Thus, this study focused on visualizing thick flakes. The thickness of the SiO_2 layer plays an important role in the visualization of a flake. Thus, for optimizing the SiO_2 thickness, the optical reflectance for a substrate with a flake was examined through calculations. In the experiment, hBN and graphite flakes were observed using a narrow band-pass filter and by differential interference contrast (DIC) microscopy. The images captured with a digital camera are discussed in terms of the color predicted from the calculation.

2. Experimental methods

2.1. Sample preparation

Figure 1(a) shows a schematic diagram of a flake consisting of a layered material placed on a SiO_2/Si substrate examined in this study. Thermally oxidized n-type Si (100) substrates, the bulk hBN crystals grown at high pressure and temperature [27], and Kish graphite (Graphene Supermarket) were used for the samples. The Si substrate with a 95 nm-thick SiO_2 layer was cleaned by sonication in acetone for 5 min and 2-propanol for 5 min. The SiO_2 thickness was adjusted to 20–77 nm by chemically etching the SiO_2 surface in a 48 wt% HF solution diluted to 5 vol% with deionized water. After exposing the substrate to UV/ozone for 15 min for clearing, single crystal thin flakes of hBN or graphite were prepared by mechanical exfoliation using scotch tape (BK-12N, Scotch) and transferred immediately to the substrate. Although the ideal isolated thick and flat flakes with the same number of layers can be obtained by the preparation, flakes that have atomic steps were focused to study the identification of the monolayer thickness difference in a flake.

2.2. Characterization

Figure 1(b) shows the setup for the optical observation of flakes on a substrate. A flake of hBN or graphite was

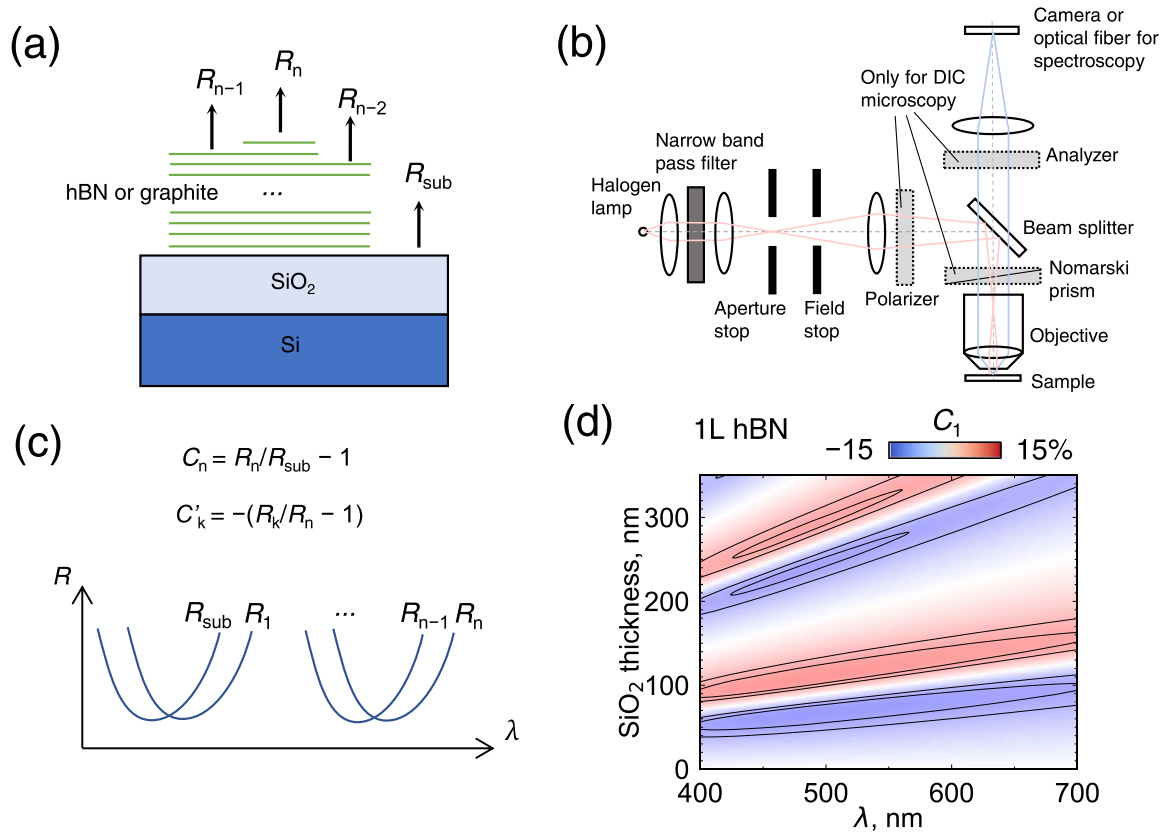

Figure 1. (a) Calculation model of a 2D flake on SiO_2/Si substrate flake with atomic thickness differences. (b) Schematic diagram of the system. (c) Schematic diagram of thickness dependence of reflectance spectra for hBN. The reflectance spectra shift to longer λ with an increase in hBN thickness. (d) Contrast of a 1 L hBN flake on SiO_2/Si substrate as a function of λ and d_{SiO2}.

observed through an objective of 50× with a numerical aperture (NA) of 0.8 (LU Plan 50×, Nikon) under light from a halogen lamp in an optical microscope (LV150, Nikon). The image was taken using a monochrome 12-bit camera (CS-63M, Bitran) cooled to 10 °C or a color 8-bit camera (EOS Kiss X4, Canon). Superior images were obtained by adjusting the aperture stop so that the light disk at the objective back focal plane was ∼80% of that for fully open. This corresponds to a substantial reduction in NA. A narrow band-pass filter was inserted in the optical path to investigate the wavelength dependence. The full width at half maximum (FWHM) of the narrow band-pass filter was 10 nm. The experimental contrast was calculated from the digital values in the image photographed by the monochrome camera [12, 15]. A flake was observed by DIC microscopy using two linear polarizers and a Nomarski prism without a narrow band-pass filter. The linear polarizers were arranged on cross Nicol. The DIC bias (Δ_0) was adjusted by changing the position of the Nomarski prism. The reflectance spectra were measured using a spectroscope (BTC-110S, B&W Tek) equipped at the trinocular head of the microscope. Since the spatial resolution of the microscopic measurement is practically less than 3 μm, the reflectance of the area only inside the flake was measured. The morphology of the substrate surface was observed by atomic force microscopy (AFM, NanoNavi, SII) with a Si cantilever (SI-DF3-R, SII Nano-Technology, Japan) in tapping mode at room temperature in ambient air (50% relative humidity, ∼20 °C). The root-mean-square roughness of the SiO_2 surface was typically 0.2 nm. The thickness of the SiO_2 film was estimated from the spectra obtained by ellipsometry (Auto SE, Horiba) and reflectance spectroscopy.

2.3. Calculation of optical contrast

The reflectance spectra and photographs were acquired through an objective lens. Therefore, the oblique incidence should be considered in the calculation. Reflectance $R(\lambda)$ at a wavelength λ is expressed as

$$R(\lambda) = \frac{1}{(\sin\theta_0)^2} \times \int_0^{\theta_0} (|r_p(\lambda,\ \theta)|^2 + |r_s(\lambda,\ \theta)|^2) \sin\theta \cos\theta d\theta \qquad (1)$$

using θ_0 is defined by $\sin\theta_0 = \mathrm{NA}$. Here $r_p(\lambda, \theta)$ and $r_s(\lambda, \theta)$ are the complex reflectivities for the p and s components of the incident light tilted from the surface normal with an angle θ, respectively [14, 18, 28–30]. NA was set to 0.7 for all calculations. $r_p(\lambda, \theta)$ and $r_s(\lambda, \theta)$ were calculated based on a multilayer model using the transfer matrix method [13]. The multilayer structure was composed of an hBN or graphite film, a SiO_2 film, and a Si substrate, as shown in figure 1(a). The refractive indices of hBN and graphite were set to 2.2 and

2.6−1.3i [9, 31] in the calculation, respectively, where i is an imaginary unit.

When the sample was photographed under a light passing through a narrow band-pass filter, the reflectance detected by the camera corresponds to the reflectance averaged for λ in the range of $\lambda' - \lambda_{\mathrm{FWHM}}/2$ to $\lambda' + \lambda_{\mathrm{FWHM}}/2$. λ' is the central wavelength of the filter, and λ_{FWHM} is the FWHM. Thus, the detected reflectance $\bar{R}(\lambda)$ can be approximated as

$$\bar{R}(\lambda) = \frac{1}{\lambda_{\mathrm{FWHM}}} \int_{\lambda' - \lambda_{\mathrm{FWHM}}/2}^{\lambda' + \lambda_{\mathrm{FWHM}}/2} R(\lambda) d\lambda. \quad (2)$$

The contrast of a flake with an n-layer thickness with regards to a substrate is defined as $C_n = R_n/R_{\mathrm{sub}} - 1$, as described in the introduction. Here, R_n is the reflectance for the flake surface, and R_{sub} is the reflectance for the surface of the substrate. Thus, the spectrum of calculated contrast is expressed as $C_n(\lambda) = \bar{R}_n(\lambda)/\bar{R}_{\mathrm{sub}}(\lambda) - 1$ [12, 15]. However, the contrast of the area with k-layer thickness in a thick flake with n-layer thickness is defined by $C_k' = -(R_k/R_n - 1)$. Similarly, the spectrum of the contrast calculated for C_k' is expressed as $C_k'(\lambda) = -(\bar{R}_k(\lambda)/\bar{R}_n(\lambda) - 1)$.

The color simulation for micrographs was performed from $R(\lambda)$. $R(\lambda)$ was converted to XYZ color space using the following equations:

$$X = \frac{K}{N} \int_{\Lambda} R(\lambda) I(\lambda) \bar{x}(\lambda) d\lambda, \quad (3a)$$

$$Y = \frac{K}{N} \int_{\Lambda} R(\lambda) I(\lambda) \bar{y}(\lambda) d\lambda, \quad (3b)$$

$$Z = \frac{K}{N} \int_{\Lambda} R(\lambda) I(\lambda) \bar{z}(\lambda) d\lambda \quad (3c)$$

where

$$N = \int_{\Lambda} I(\lambda) \bar{y}(\lambda) d\lambda, \quad (3d)$$

$\bar{x}(\lambda)$, $\bar{y}(\lambda)$, and $\bar{z}(\lambda)$ are the CIE color matching functions; Λ denotes the integration on [380 nm, 780 nm]; $I(\lambda)$ is the illuminant; K is a constant. The light source of a halogen lamp was assumed to be black-body radiation of 3500 K. K is adjusted and is proportional to the exposure time to reproduce the photograph. The X, Y, and Z values are converted to the standard RGB values.

3. Results and discussion

Figure 1(c) presents a schematic diagram of the R_{sub}, R_1, R_{n-1}, and R_n spectra for a flake with an n-layer thickness shown in figure 1(a). The wavelength at which the spectrum has the minimum shifts to a long wavelength as the atomic layer thickness is increased [17, 18]. This study focused on visualizing a hBN flake rather than a graphite flake. This is because the visualization of a hBN flake, which is optically transparent, is more complex than that of a graphite flake, which is not transparent. First, the contrast for a 1 L hBN flake on a SiO_2/Si substrate was examined to visualize areas with a 1 L difference in a thick hBN flake discussed below. Figure 1(d) shows the contrast calculated for a 1 L hBN flake on SiO_2/Si substrate (C_1) as a function of λ and SiO_2 thickness (d_{SiO2}) [10]. As defined in section 2.3, the contrast is given by $C_1 = R_1/R_{\mathrm{sub}} - 1$. On a SiO_2 film with a thickness of 60–140 nm or 260–330 nm, the contrast is approximately ±3% at a certain λ [9].

The contrast for a thick hBN flake was next examined. In particular, this study focused on the contrast of a hBN flake with $d_{\mathrm{BN}} = 40$ nm ($n = 120$) as an example. Figure 2(a) shows the C_n calculated as a function of d_{BN} and λ for $d_{\mathrm{SiO2}} = 90$ nm. The C_n increased as d_{BN} was increased and reached the maximum at $d_{\mathrm{BN}} = \sim$60 nm since the R_{sub} is constant, which was attributed to the increase in R_n. For $d_{\mathrm{BN}} = 40$ nm, R_{sub}, R_{120}, and C_{120} are calculated to be 11.13%, 58.59%, and 426.6% at $\lambda = 500$ nm, respectively. A hBN flake of $d_{\mathrm{BN}} = 40$ nm in an image taken at $\lambda = 500$ nm should be brighter than the substrate on which the flake is placed since C_{120} is a positive value. Ifthe flake has an area of 1 L thinner, R_{119} and C_{119} are 58.38% and 424.8%, respectively. The difference of R_{120} and R_{119} was 0.21%, which was 0.0037 of $R_{120} = 58.59\%$. Thus, it is difficult to visualize a 1 L difference if a general 8-bit camera with linear sensitivity to light intensity is used. The difficulty is explained as follows. An 8-bit data image gives 256 shades expressed by digital integers (D) of 0 to 255. The D is a value of $ctI(\lambda)R(\lambda)$ as an integer where c is a camera constant, and t is the exposure time. The value of $(R_{120} - R_{119})/R_{120}$, 0.0037, is close to $0.0039 = 1/256$. Therefore, the D value for R_{119} is equal to or one less than that for R_{120}. This causes difficulty in visualization. As described in section 2.3, $-(R_{\mathrm{k}}/R_{\mathrm{n}} - 1)$ is suitable for quantitatively evaluating the difference in atomic layer thickness in a flake. Thus, the contrast for the difference in atomic layer thickness in a thick flake is defined as $C_k' = -(R_k/R_n - 1)$. According to the definition, the contrast of a 1 L thickness difference is expressed as $C'_{n-1} = -(R_{n-1}/R_n - 1)$. Figure 2(b) shows the C'_{n-1} calculated as a function of d_{BN} and λ for $d_{\mathrm{SiO2}} = 90$ nm. For $d_{\mathrm{BN}} = 40$ nm, the C'_{120-1} value was 0.37% at $\lambda = 500$ nm. Figures 2(a) and (b) show that a SiO_2/Si substrate of $d_{\mathrm{SiO2}} = 90$ nm is suitable for visualizing a thick flake. In contrast, the SiO_2/Si substrate is unsuitable for confirming the area with the difference in atomic layer thickness in the flake. Figures 2(c) and (d) show the C_n and C'_{n-1} for 20 nm-thick SiO_2 as a function of d_{BN} and λ. The C_n value for 20 nm-thick SiO_2 is lower than that for 90 nm-thick SiO_2 over a wide range, including $d_{\mathrm{BN}} = 40$ nm. In contrast, the absolute value of C'_{n-1} for a 20 nm-thick SiO_2 is larger than that for a 90 nm-thick SiO_2 over a wide range. In particular, the C'_{120-1} value was 12.2% at $\lambda = 500$ nm. The small R_{120} value of 0.78% contributes to the large C'_{120-1}. In addition, the C_{120} value was 98% at $\lambda = 500$ nm, and a hBN flake of $d_{\mathrm{BN}} = \sim$40 nm should be observed. Thus, a SiO_2/Si substrate of $d_{\mathrm{SiO2}} = 20$ nm is suitable for visualizing the area with the difference in atomic layer thickness in the flake.

As the calculation results in the above paragraph, R_{sub} and R_n are essential factors for visualizing a flake and an area with the difference in atomic layer thickness in the flake, respectively. Thus, the spectra of R_{sub} and R_n were measured experimentally. Figure 3 shows the spectra of R_{sub} and R_n obtained from measurement and calculation. The calculation

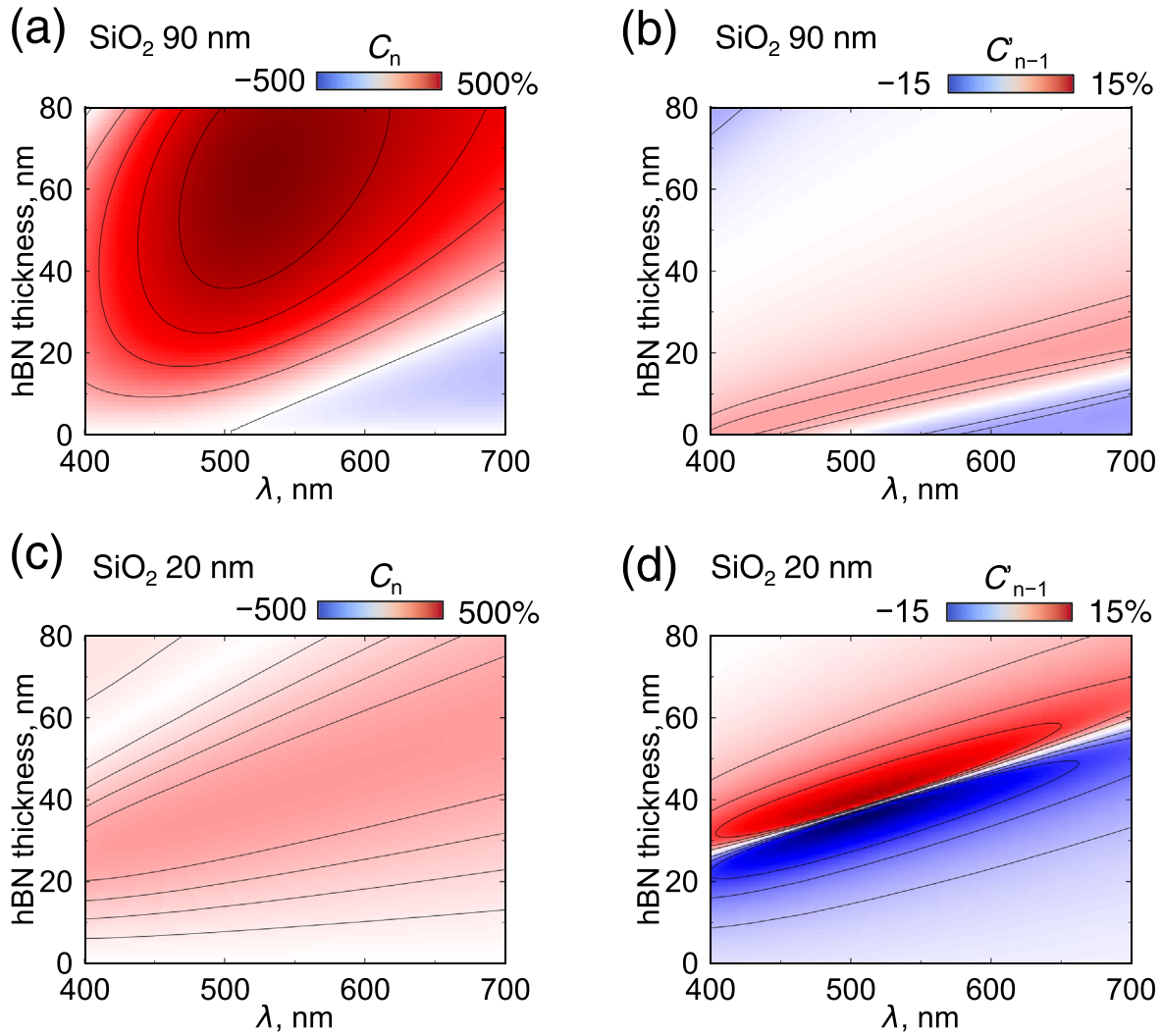

Figure 2. Contrast as a function of d_{BN} and λ. (a) and (b) present C_n and C'_{n-1} for $d_{SiO2} = 90$ nm, respectively. (c) and (d) present C_n and C'_{n-1} for $d_{SiO2} = 20$ nm, respectively.

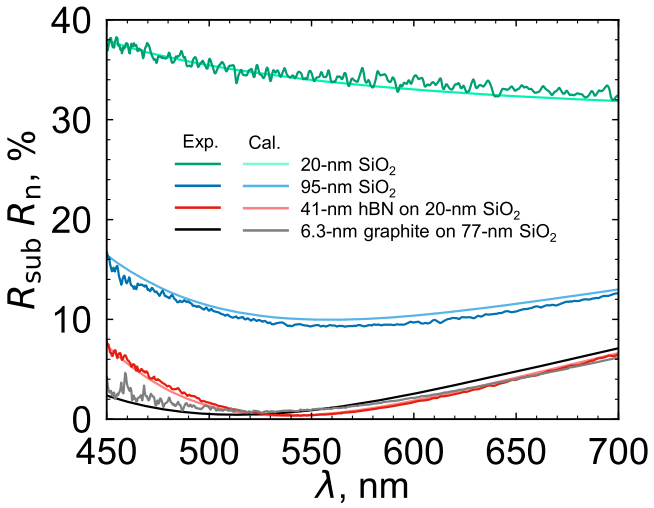

Figure 3. Reflectance spectra of R_{sub} with different d_{SiO2} and R_n for hBN and graphite. The solid lines of light and dark colors indicate the experiment and calculation, respectively. R_n for a thick hBN and graphite flake on the optimized SiO_2/Si substrate is close to zero at certain λ.

results indicated by the light colors roughly reproduce the experimental spectra for all cases. The solid dark green and blue lines in the figure indicate R_{sub} for $d_{SiO2} = 20$ nm and 95 nm, respectively. R_{sub} for the 95 nm SiO_2 film was smaller than that for the 20 nm SiO_2 film, as shown in figure 3. The red and black lines show R_n for 41 nm hBN on a 20 nm SiO_2 film and 6.3 nm graphite on a 77 nm SiO_2 film, respectively. The SiO_2 thickness was optimized to realize small R_n. R_n for a thick hBN and a graphite flake on the optimized SiO_2/Si substrate is close to zero at a certain λ.

Figure 4 presents the results obtained for a 45 nm (136 L) hBN flake on a 20 nm SiO_2 film by optical microscopy and AFM. Figure 4(a) is a color image taken under white light. A flake with a navy-blue color was observed. Figure 4(b) is a monochromatic image taken under light passing through a band-pass filter of $\lambda = 530$ nm, corresponding to the dotted area in figure 4(a). Some steps are shown in figure 4(b). This result indicates that using an appropriate band-pass filter contributes to the visualization of steps. In addition, the exposure time for capturing the image was adjusted for R_n,

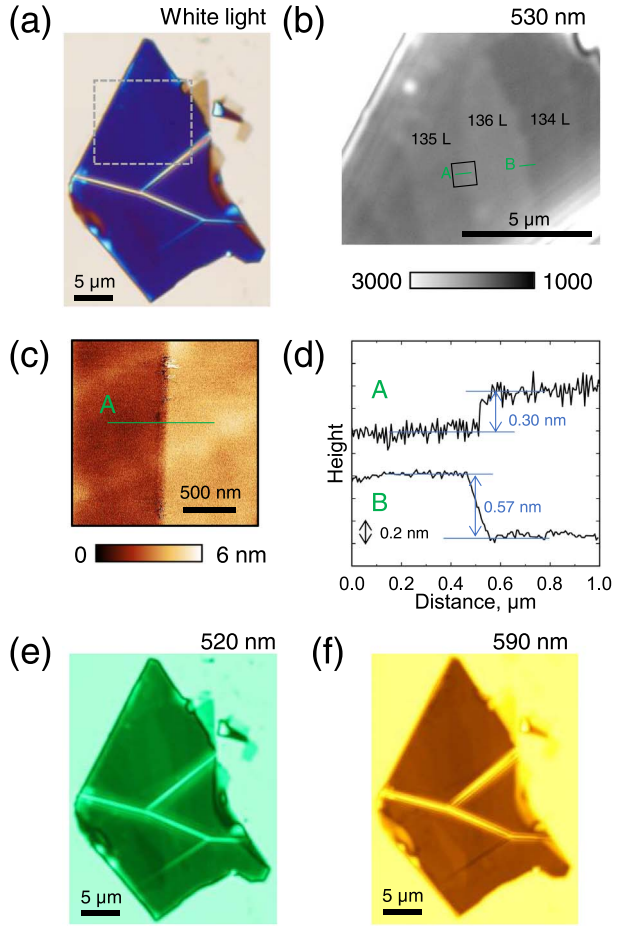

Figure 4. Characterization of a 45 nm hBN flake on 20 nm SiO_2 film. (a) Color photograph with white light. (b) Monochromatic image at $\lambda = 530$ nm, which corresponds to the dotted area in (a). (c) AFM height image corresponding to the black line area in (b). (d) Height profile along the solid green lines in (b) or (c). (e) and (f) Color photographs at $\lambda = 520$ and 590 nm, respectively.

being different from that for R_{sub} since R_{sub} is higher than R_n. As a result, the D of the area of the substrate saturates and is fully white in the image. Figure 4(c) shows an AFM height image corresponding to the area enclosed by the solid black line in figure 4(b). Figure 4(d) shows the two height profiles along the green lines labeled A and B in figure 4(b). The step height is 0.30 nm and 0.57 nm for lines A and B, respectively, corresponding to the thicknesses of 1 L and 2 L, respectively. Thus, the downside area for lines A and B is an area of $n = 135$ and 134, respectively. Figure 4(b) presents the measured n values. The steps can be recognized in an image taken using a commercial color camera. Figures 4(e) and (f) show color images observed under light through a band-pass filter of $\lambda = 520$ and 590 nm, respectively. These images have not been processed by software. For $\lambda = 520$ nm, the area of 136 L has a bright color compared with the surrounding area. For $\lambda = 590$ nm, the area of 136 L has a dark color compared with the surrounding area. The brightness and darkness are explained by C'_{n-1}, as shown in figure 2(d). At $d_{BN} = 45$ nm, the C'_{n-1} value is positive at $\lambda = 520$ nm and negative at $\lambda = 590$ nm, corresponding to the brightness and darkness, respectively.

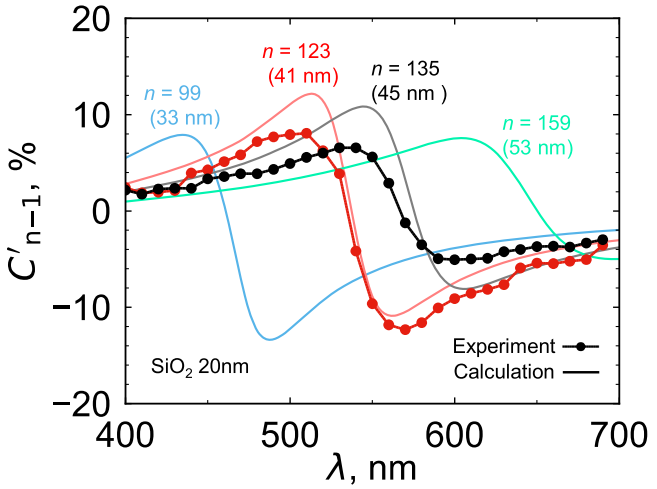

Figure 5. Contrast spectra of C'_{n-1} of different d_{BN} for $d_{SiO2} = 20$ nm. The dots and solid lines indicate the experiment and calculation, respectively.

Figure 5 shows the C'_{n-1} spectra for $d_{SiO2} = 20$ nm obtained by measurements and calculations. The red and black plots represent the experimental spectra for $d_{BN} = 41$ nm and 45 nm, respectively. The solid lines with a light color, by calculation, roughly reproduce the experimental spectra. The difference between calculation and experimental spectra may be caused by scattering light from the surrounding thick flake. For $d_{BN} = 41$ nm, the experimental spectrum has the maximum $|C'_{n-1}|$ of 12% at 570 nm. The C'_{n-1} value for a 1 L difference in thickness is comparable to the contrast of a 1 L hBN flake on the antireflection of silicon nitride substrate [14]. When a desirable flake is found from a large amount of exfoliated flakes on a substrate, the flake often has small fragments or tape residues on the surface. The present technique can also visualize them (figure S1).

For figure 5, the SiO_2 thickness, d_{SiO2}, is fixed at 20 nm. Next, the dependence of d_{SiO2} on C'_{n-1} based on calculation results for the realization of a large contrast was investigated. The maximum $|C'_{n-1}|$ in a wavelength range is used to evaluate the contrast since the C'_{n-1} value depends on λ. The observation of a flake is often conducted in a visible wavelength range using a halogen lamp. Thus, the maximum $|C'_{n-1}|$ was defined in the range of 450–750 nm as the maximum contrast, C'_{max}. The wavelength range of $\lambda <$ 450 nm was excluded because of the low luminance of a halogen lamp and the low sensitivity of a common camera in the range.

Figure 6(a) shows C'max calculated as a function of d_{SiO2} and d_{BN}. A contour map is useful for optimizing d_{SiO2} so a flat hBN flake with a desirable thickness can be found. For example, the optimized d_{SiO2} for a thick hBN flake with $d_{BN} = \sim 40$ nm is approximately 20 nm. Thus, SiO_2/Si substrates of $d_{SiO2} = 20$ nm were used in the experiment, as shown in figures 4 and 5. The λ for the maximum $|C'_{n-1}|$ depends on d_{SiO2} and d_{BN}, where the white dotted lines indicate the contour lines. The dependence of λ is shown in figure S2. The map of the λ exhibits discontinuity since λ for

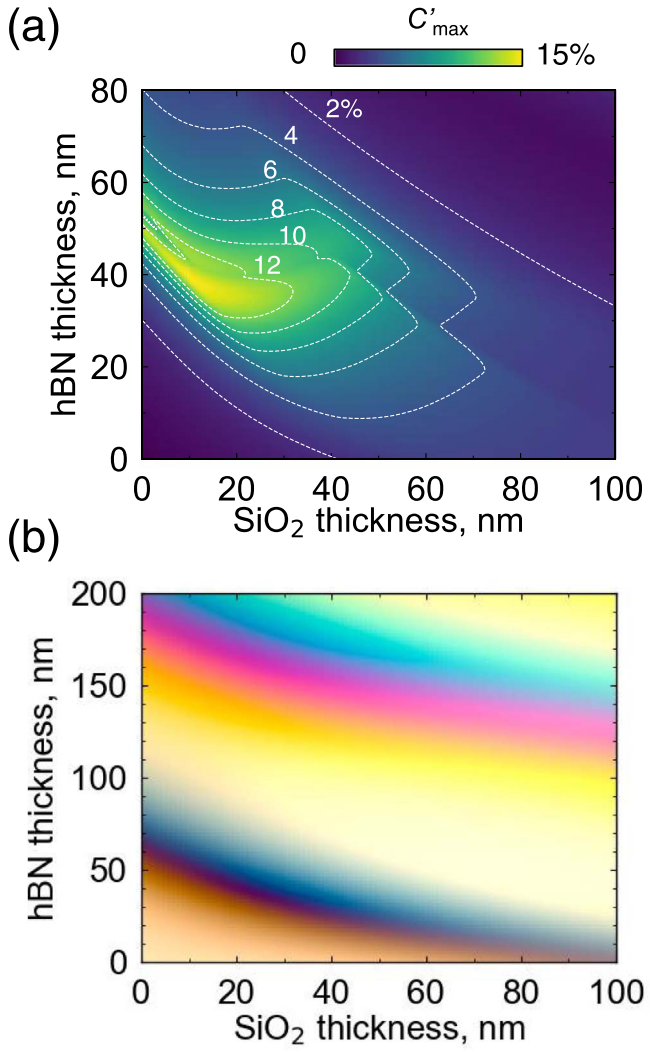

Figure 6. (a) Maximum $|C'_{n-1}|$ in the range of 450–750 nm as a function of d_{BN} and d_{SiO2}. (b) Color simulation of hBN on a SiO_2/Si substrate as a function of d_{BN} and d_{SiO2}.

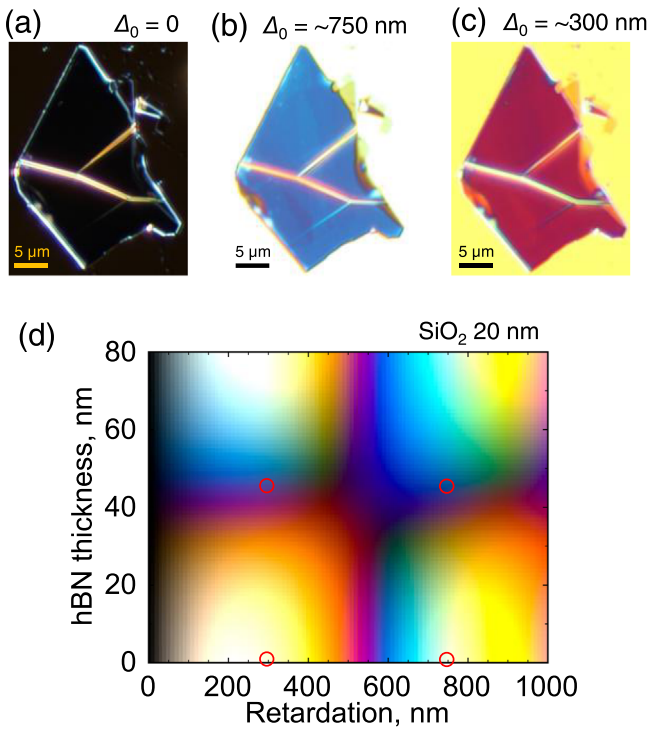

Figure 7. DIC microscopy of a 45 nm hBN flake on 20 nm SiO_2 film. DIC photographs at $\Delta_0 = 0$ (a), 750 (b), and 300 nm (c). The flake is the same as for figure 4. The atomic steps are visualized in DIC microscopy without a band-pass filter by appropriate DIC bias. (d) Color simulation of hBN in the DIC image for $d_{SiO2} = 20$ nm as a function of d_{BN} and Δ_0.

C'_{max} is limited in the range of 450–750 nm. Figure S3 shows the C'_{n-1} spectra for a certain d_{BN}.

A consumer color camera is often used when a hBN flake with a desirable thickness is found. The color in an image of a hBN flake captured by a color camera can be predicted by calculations. Such a predicted color is useful for finding a hBN flake. Figure 6(b) represents a color map calculated for a hBN flake on a SiO_2/Si substrate as a function of d_{BN} and d_{SiO2}. The color gradually changes with d_{BN} and d_{SiO2}. The color at $d_{BN} = 0$ corresponds to that of the SiO_2/Si substrate. For example, the color for $d_{SiO2} = 20$ nm is a wheat color at $d_{BN} = 0$ and a navy color at $d_{BN} = 45$ nm. The thickness corresponds to the sample shown in figure 4(a). The calculated color roughly reproduces the color in the image captured with the actual digital camera. The data of C'_{max} and color simulation of hBN for thicker SiO_2 are shown in figure S4.

A narrow band-pass filter enables the visualization of a 1 L thickness difference in a thick hBN flake, as shown in figure 4(b). In this technique, a band-pass filter with the appropriate λ for d_{BN} of a hBN flake was selected. Another technique that does not require a narrow band-pass filter was proposed. A DIC microscope also enables the visualization of 1 L thickness difference. Figure 1(b) presents the setup for DIC microscopy. The optical components installed on a commercial reflected microscope were used for DIC microscopy.

Figures 7(a)–(c) shows an image of a 45 nm hBN flake on 20 nm SiO_2 film observed under white light using a DIC microscope with different DIC bias, Δ_0. The flake is the same as that for figure 4. The observed color of the flake and substrate depends on Δ_0, which an operator can adjust. The color of the flake is black for $\Delta_0 = 0$, blue for $\Delta_0 = \sim 750$ nm, and wine-red for $\Delta_0 = \sim 300$ nm. Figures 7(b) and (c) show that the flake has some areas colored with different colors shown in figures 4(e) and (f). This result indicates the presence of atomic steps.

Generally, DIC microscopy converts the gradient (Δ_1) of the refractive index and/or the optical path length in an observation specimen into intensity in an image. Therefore, when a thick hBN flake on a substrate is observed by DIC microscopy, edges with thickness differences are highlighted in an image. The flake and substrate colors are black in figure 7(a) for $\Delta_0 = 0$. By contrast, the edges of thickness difference for the flake and wrinkles are highlighted by the white and yellow lines because of the large Δ_1, respectively. Therefore, the shape of the thick hBN flake is recognized by the white shape outlines. However, the presence of atomic steps cannot be recognized in the image since the highlighted

lines of the atomic step edge were not observed. This result suggests that Δ_1 of 1 L hBN is insufficient to change the intensity in the DIC image.

DIC bias colorizes the flake and substrate in addition to the highlighted lines of the thickness difference. The color of the flake and substrate in figure 7(c) for $\Delta_0 = \sim$300 nm is wine-red and yellow, respectively. Furthermore, the edges of large thickness differences are also highlighted in the image. The white edge lines in figure 7(a) were changed to green by the DIC bias in figure 7(c). These colors that depend on Δ_0 are interference colors. In addition, DIC bias visualizes the atomic steps. Unlike the steps of large thickness difference, the presence of atomic steps can be recognized in figures 7(b) and (c) by the color difference, not outlines (figure S5). In this case, the color difference in atomic steps might be attributed to the sum of differences in $R(\lambda)$ at various λ, as shown in figures 1 and 2. Thus, the color of the substrate and flake were simulated. The intensity of each λ is dominated by Δ_0 and $R(\lambda)$, where the effect of Δ_1 is included in $R(\lambda)$. The light intensity detected by a camera, $I_{\mathrm{DIC}}(\lambda, \Delta_0)$, can be expressed by [32]

$$I_{\mathrm{DIC}}(\lambda, \Delta_0) = ctI_0(\lambda)R(\lambda)\sin^2(\pi\Delta_0/\lambda). \quad (4)$$

The light intensity with λ is zero at $\Delta_0 = \lambda l$ ($l = 0, 1, 2, \ldots$). Therefore, a Nomarski prism is an optical component that continuously tunes the light source spectrum with a trigonometric function by the DIC bias. Consequently, images of a flake with colors depending on atomic layer thickness were obtained by adjusting the DIC bias instead of using a band-pass filter.

Figure 7(d) shows the color simulation of hBN in the DIC image for $d_{\mathrm{SiO2}} = 20$ nm as a function of d_{BN} and Δ_0. The color for $d_{\mathrm{BN}} = 0$ corresponds to that for the substrate. The color was obtained using equation (4). The colors corresponding to the substrate and the hBN flake in figures 7(b) and (c) are marked with red circles. The colors obtained by the calculation are approximately the experimental colors in figures 7(b) and (c). The DIC bias of Δ_0 enhances the light of $\lambda = \Delta_0/(l + 1/2)$ and weakens the light of $\lambda = \Delta_0/l$. The DIC bias of 750 and 300 nm enhances 500 and 600 nm light, respectively. The enhanced of $\lambda = 500$ nm is close to the wavelength of 540 nm for the maximum positive contrast in figure 5. Consequently, the camera at $\Delta_0 = 750$ nm mainly detects light in the range of the positive contrast and generates a similar image of figure 4(e). Similarly, the image at $\Delta_0 = 300$ nm can be explained.

A similar investigation with a hBN flake on a SiO_2/Si substrate of $d_{\mathrm{SiO2}} = 20$ nm was also conducted for a graphite flake on a SiO_2/Si substrate of $d_{\mathrm{SiO2}} = 77$ nm. Figures 8(a) and (b) show the photographs of a graphite flake with areas of various thicknesses taken under white light and $\lambda = 490$ nm illumination, respectively. For the flake, the minimum difference in the atomic layer thickness was 2 L. The step on the surface of the graphite was observed compared with that of the hBN flake with a 2 L difference in figure 4(b). The clear observation was attributed to the extinction coefficient in the refractive index of graphite [9]. Figure 8(c) shows the contour map of C'_{n-1} for 77 nm SiO_2 film as a function of d_{BN} and λ. The $|C'_{n-1}|$ value for graphite is larger than that for hBN. The C'_{n-1} for $d_{\mathrm{gra}} > 5.5$ nm and $d_{\mathrm{gra}} < 5.5$ nm is positive and negative at $\lambda = 490$ nm, respectively. This explains the contrast pattern in figure 8(b), where the brightness at the position of 14 L (4.66 nm) and 20 L (6.66 nm) is higher than that of 16 L (5.33 nm) and 18 L (6.00 nm). Note that the positive and negative contrast region in the contour map for C'_{n-2} is similar to that for C'_{n-1} (figure S6). Figure 8(d) shows the experimental C'_{n-1} spectrum for the different graphite flake of $d_{\mathrm{gra}} = 4.66$ nm having a 1 L thickness difference with calculations. The black dots for the experiment indicate an enhancement of the contrast of 33% at $\lambda = 510$ nm, which is reproduced with the calculation represented with the solid line. Figure 8(e) shows the calculated $C'_{\max}$ as a function of d_{gra} and d_{SiO2}. The SiO_2/Si substrate of $d_{\mathrm{SiO2}} = \sim$75 nm is suitable for finding a flat graphite flake with $d_{\mathrm{gra}} = \sim$5 nm. Figure 8(f) shows the simulated color for graphite on SiO_2/Si substrate as a function of d_{gra} and d_{SiO2}. The color of the graphite and substrate is approximated with the simulation.

4. Conclusions

We attempted the visualization of thick hBN and graphite flakes on SiO_2/Si substrates, particularly the area with different thicknesses. The reflectance of a thick flake on SiO_2/Si substrate depends on the SiO_2 thickness, and approaches zero at a certain λ by adjusting the SiO_2 thickness with respect to the flake thickness. The reflectances of 41 nm hBN on 20 nm SiO_2 and 6.3 nm graphite on 77 nm SiO_2 were close to zero at $\lambda = \sim$530 nm. At the wavelength that the reflectance from an area of a flake is close to zero, the contrast is sensitive to the thickness difference. Therefore, the difference in the atomic layer thickness in the flake was visualized. The contrast spectra of a 1 L thickness difference were measured using narrow band-pass filters of various λ. The maximum absolute contrast measured for a 1 L difference in thickness was 12% and 33% for 41 nm hBN on 20 nm SiO_2 at $\lambda = 570$ nm and 4.3 nm graphite on 77 nm SiO_2 at $\lambda = 510$ nm, respectively. The high contrast is sufficient to evaluate the atomic thickness difference with a consumer eight-bit color camera.

A rapid inspection technique that does not use a band-pass filter was proposed. Using the conventional setup of DIC microscopy, the same h-BN flake on 20 nm SiO_2 film was observed under white light illumination. The colors of the substrate and flakes in the DIC image are determined mainly by the DIC bias and $R(\lambda)$ because of the small difference in the optical path length corresponding to the 1 L difference in thickness in the flake. In this case, DIC bias serves as an adjustable band-pass filter and restricts a light source spectrum to the wavelength determined by a trigonometric function. Therefore, the differences in atomic thickness were visualized similarly because of the sum of the difference in $R(\lambda)$ for various λ. The colors of the substrate and flake in the photographed image were approximated by the calculation.

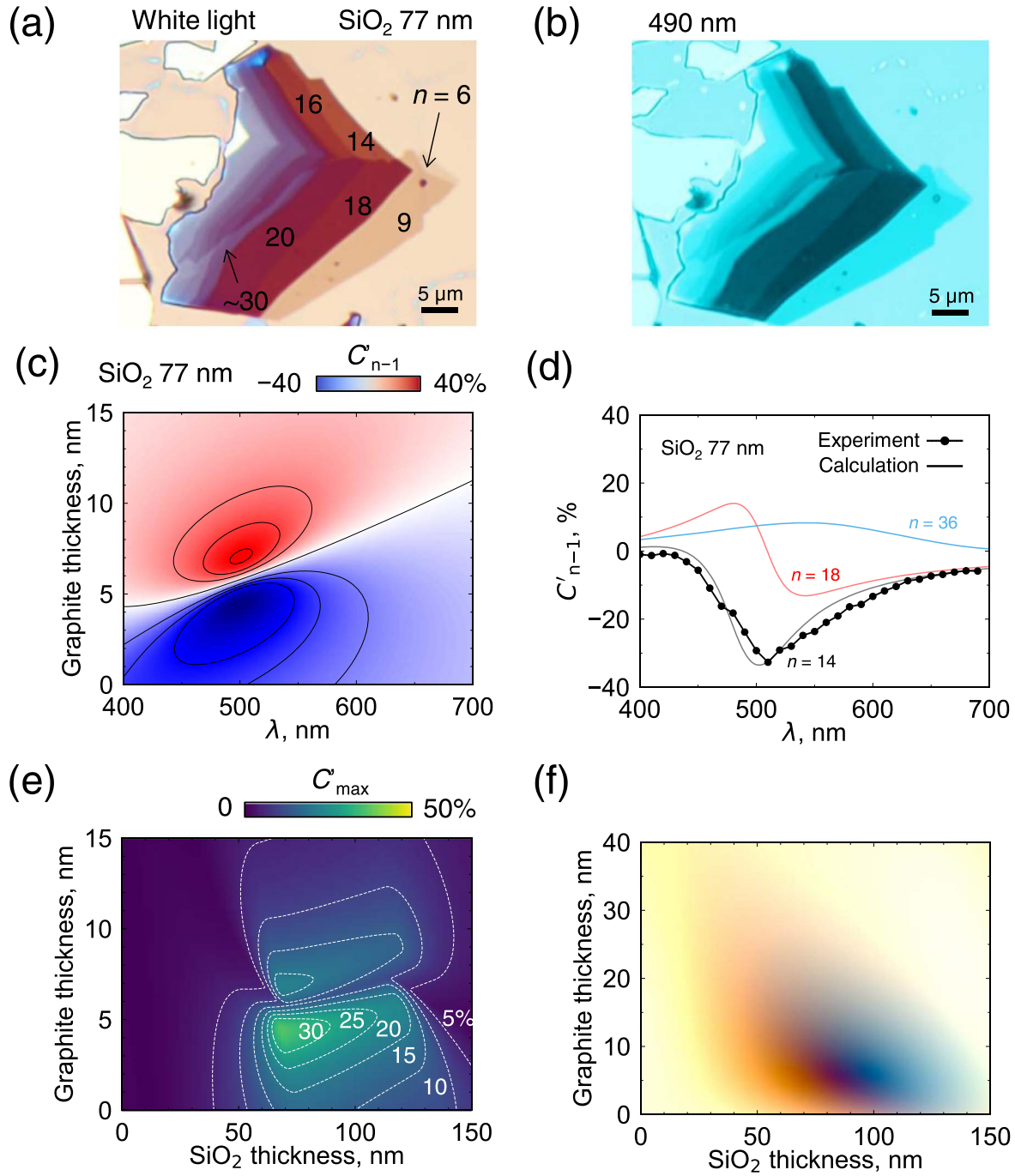

Figure 8. Characterization of the graphite flake on 77 nm SiO_2 film. (a) and (b) Color photograph of white light and $\lambda = 490$ nm, respectively. The numbers in (a) indicate the layer number. (c) C'_{n-1} as a function of d_{BN} and λ for $d_{SiO2} = 77$ nm. (d) Contrast spectra of C'_{n-1} of different d_{Gra} for $d_{SiO2} = 77$ nm. The dots and solid lines indicate experiment and calculation, respectively. (e) Maximum $|C'_{n-1}|$ in the range of 450–750 nm as a function of d_{Gra} and d_{SiO2}, where the white dotted lines indicate the contour lines. (f) Color simulation of graphite on SiO_2/Si substrate as a function of d_{Gra} and d_{SiO2}.

Generally, thick exfoliated flakes used for van der Waals heterostructures are obtained on a Si substrate with a ~90 or ~300 nm SiO_2 layer. This study shows that optimizing the SiO_2 thickness instead of using a SiO_2 layer with such a thickness contributes to selecting a desirable flake from a large number of exfoliated flakes on the substrate. The SiO_2 thicknesses optimized for ~40 nm hBN and ~5 nm graphite was ~20 and ~75 nm, respectively. The hBN and graphite flakes had purple and dark red-purplish colors in the digital camera image. The proposed observation technique is useful for constructing ideal van der Waals heterostructures.

Acknowledgments

This work was partly supported by JSPS KAKENHI Grant Numbers 21K04195, 21H04655, Kansai Research Foundation, Chubei Itoh Foundation, Iketani Science and

Technology Foundation, and Hyogo Science and Technology Association.

Data availability statement

All data that support the findings of this study are included within the article (and any supplementary files).

ORCID iDs

Yoshiaki Hattori https://orcid.org/0000-0002-5400-8820
Kenji Watanabe https://orcid.org/0000-0003-3701-8119
Masatoshi Kitamura https://orcid.org/0000-0003-1342-4796

References

[1] Yao J D and Yang G W 2021 All-2D architectures toward advanced electronic and optoelectronic devices *Nano Today* **36** 101026
[2] Wang L, Huang L, Tan W C, Feng X, Chen L, Huang X and Ang K-W 2018 2D photovoltaic devices: progress and prospects *Small Methods* **2** 1700294
[3] Zhou Y, Xu W, Sheng Y, Huang H, Zhang Q, Hou L, Shautsova V and Warner J H 2019 Symmetry-controlled reversible photovoltaic current flow in ultrathin All 2D vertically stacked graphene/MoS_2/WS_2/graphene devices *ACS Appl. Mater. Interfaces* **11** 2234–42
[4] Balaji Y, Smets Q, Szabo Á, Mascaro M, Lin D, Asselberghs I, Radu I, Luisier M and Groeseneken G 2020 MoS_2/$MoTe_2$ Heterostructure Tunnel FETs Using Gated Schottky Contacts *Adv. Funct. Mater.* **30** 1905970
[5] Lee K-C *et al* 2019 Analog circuit applications based on All-2D ambipolar $ReSe_2$ field-effect transistors *Adv. Funct. Mater.* **29** 1809011
[6] Chuang H-J, Chamlagain B, Koehler M, Perera M M, Yan J, Mandrus D, Tománek D and Zhou Z 2016 Low-resistance 2D/2D ohmic contacts: a universal approach to high-performance WSe_2, MoS_2, and $MoSe_2$ transistors *Nano Lett.* **16** 1896–902
[7] Mukherjee B, Zulkefli A, Watanabe K, Taniguchi T, Wakayama Y and Nakaharai S 2020 Laser-assisted multilevel non-volatile memory device based on 2D van-der-Waals few-layer-ReS_2/h-BN/graphene heterostructures *Adv. Funct. Mater.* **30** 2001688
[8] Novoselov K S, Geim A K, Morozov S V, Jiang D, Zhang Y, Dubonos S V, Grigorieva I V and Firsov A A 2004 Electric field effect in atomically thin carbon films *Science* **306** 666–9
[9] Blake P, Hill E W, Castro Neto A H, Novoselov K S, Jiang D, Yang R, Booth T J and Geim A K 2007 Making graphene visible *Appl. Phys. Lett.* **91** 063124
[10] Gorbachev R V *et al* 2011 Hunting for monolayer boron nitride: optical and raman signatures *Small* **7** 465–8
[11] Donnelly G E, Velický M, Hendren W R, Bowman R M and Huang F 2020 Achieving extremely high optical contrast of atomically-thin MoS_2 *Nanotechnology* **31** 145706
[12] Hattori Y, Taniguchi T, Watanabe K and Kitamura M 2021 Visualization of a hexagonal boron nitride monolayer on an ultra-thin gold film via reflected light microscopy *Nanotechnology* **33** 065702
[13] Casiraghi C, Hartschuh A, Lidorikis E, Qian H, Harutyunyan H, Gokus T, Novoselov K S and Ferrari A C 2007 Rayleigh imaging of graphene and graphene layers *Nano Lett.* **7** 2711–7
[14] Huang F 2019 Optical contrast of atomically thin films *J. Phys. Chem.* C **123** 7440–6
[15] Hattori Y, Taniguchi T, Watanabe K and Kitamura M 2022 Enhancement of the contrast for a hexagonal boron nitride monolayer placed on a silicon nitride/silicon substrate *Appl. Phys. Express* **15** 086502
[16] Syahir A, Mihara H and Kajikawa K 2010 A new optical label-free biosensing platform based on a metal−insulator−metal structure *Langmuir* **26** 6053–7
[17] Hattori Y, Takahashi H, Ikematsu N and Kitamura M 2021 Chain-length dependence of optical properties for an alkanethiol monolayer on an ultrathin gold film revealed via reflected light microscopy *J. Phys. Chem.* C **125** 14991–9
[18] Hattori Y and Kitamura M 2023 Reflected light microscopy of a gold oxide layer formed on a Au film by ultraviolet/ozone treatment *Thin Solid Films* **764** 139631
[19] Rubio-Bollinger G, Guerrero R, De Lara D P, Quereda J, Vaquero-Garzon L, Agraït N, Bratschitsch R and Castellanos-Gomez A 2015 Enhanced visibility of MoS_2, $MoSe_2$, WSe_2 and black-phosphorus: making optical identification of 2D semiconductors easier *Electronics* **4** 847–56
[20] An J Y and Kahng Y H 2018 Optical observation of single layer graphene on silicon nitride substrate *AIP Adv.* **8** 015107
[21] Wang L *et al* 2013 One-dimensional electrical contact to a two-dimensional material *Science* **342** 614–7
[22] Bresnehan M S, Hollander M J, Wetherington M, LaBella M, Trumbull K A, Cavalero R, Snyder D W and Robinson J A 2012 Integration of hexagonal boron nitride with quasi-freestanding epitaxial graphene: toward wafer-scale, high-performance devices *ACS Nano* **6** 5234–41
[23] Tang J *et al* 2020 Vertical integration of 2D building blocks for All-2D electronics *Adv. Electron. Mater.* **6** 2000550
[24] Wu L *et al* 2020 InSe/hBN/graphite heterostructure for high-performance 2D electronics and flexible electronics *Nano Res.* **13** 1127–32
[25] Lembke D, Bertolazzi S and Kis A 2015 Single-layer MoS_2 electronics *Acc. Chem. Res.* **48** 100–10
[26] Albarakati S *et al* 2019 Antisymmetric magnetoresistance in van der Waals Fe_3GeTe_2/graphite/Fe_3GeTe_2 trilayer heterostructures *Sci. Adv.* **5** eaaw0409
[27] Watanabe K, Taniguchi T and Kanda H 2004 Direct-bandgap properties and evidence for ultraviolet lasing of hexagonal boron nitride single crystal *Nature Mater* **3** 404–9
[28] Katzen J M, Velický M, Huang Y, Drakeley S, Hendren W, Bowman R M, Cai Q, Chen Y, Li L H and Huang F 2018 Rigorous and accurate contrast spectroscopy for ultimate thickness determination of micrometer-sized graphene on gold and molecular sensing *ACS Appl. Mater. Interfaces* **10** 22520–8
[29] Li X-L, Qiao X-F, Han W-P, Zhang X, Tan Q-H, Chen T and Tan P-H 2016 Determining layer number of two-dimensional flakes of transition-metal dichalcogenides by the Raman intensity from substrates *Nanotechnology* **27** 145704
[30] Lu Y, Li X-L, Zhang X, Wu J-B and Tan P-H 2015 Optical contrast determination of the thickness of SiO_2 film on Si substrate partially covered by two-dimensional crystal flakes *Sci. Bull.* **60** 806–11
[31] Ohba N, Miwa K, Nagasako N and Fukumoto A 2001 First-principles study on structural, dielectric, and dynamical properties for three BN polytypes *Phys. Rev.* B **63** 115207
[32] Sørensen B E 2013 A revised Michel-Lévy interference colour chart based on first-principles calculations *Eur. J. Mineral.* **25** 5–10